Spiking attractor model of motor cortex explains modulation of neural and behavioral variability by prior target information

Vahid Rostami
Computational Systems Neuroscience, Institute of Zoology, University of Cologne
Thomas Rost
Computational Systems Neuroscience, Institute of Zoology, University of Cologne
Alexa Riehle
Institut de Neurosciences de la Timone https://orcid.org/0000-0001-5890-3999
Sacha van Albada
FZ Juelich https://orcid.org/0000-0003-0682-4855
Martin Nawrot (mnawrot@uni-koeln.de)
Computational Systems Neuroscience, Institute of Zoology, University of Cologne

Article

Keywords:

Posted Date: April 1st, 2022

DOI: https://doi.org/10.21203/rs.3.rs-1337724/v1

Spiking attractor model of motor cortex explains modulation of neural and behavioral variability by prior target information

Vahid Rostami*[1], Thomas Rost*[1], Alexa Riehle[2,3], Sacha J. van Albada[3,4,5], Martin P. Nawrot[1]

1 Computational Systems Neuroscience, Institute of Zoology, University of Cologne, Cologne, Germany

2 UMR7289 Institut de Neurosciences de la Timone (INT), Centre National de la Recherche Scientifique (CNRS)—Aix-Marseille Université (AMU), Marseille, France

3 Institute of Neuroscience and Medicine (INM-6), Jülich Research Center, Jülich, Germany

4 Institute for Advanced Simulation (IAS-6) and JARA Institute Brain Structure-Function Relationships (INM-10), Jülich Research Center, Jülich, Germany

5 Computational Neuroanatomy, Institute of Zoology, University of Cologne, Cologne, Germany

Correspondence: martin.nawrot@uni-koeln.de

Abstract

When preparing a movement, we often rely on partial or incomplete information, which can decrement task performance. In the behaving monkey we show that the degree of cued target information is reflected in both, neural variability in motor cortex and behavioral reaction times. We study the underlying mechanisms in a spiking motor-cortical attractor model. By introducing a novel and biologically realistic network topology where excitatory neuron clusters are locally balanced with inhibitory neuron clusters we robustly ensure multistable network activity across a wide range of network parameters. In application to the monkey task, the model performs target selection and accurately reproduces the task-epoch dependent reduction of trial-to-trial variability in vivo where the degree of reduction directly reflects the amount of available target information, while spiking irregularity remained constant throughout the task. In the context of incomplete cue information, the increased target selection time of the model explains the increased behavioral reaction time of the monkey. We conclude that context-dependent neural and behavioral variability are a signum of attractor computation in the motor cortex.

1 Introduction

Despite correct motor performance in well-trained animals, behavioral reaction times and neural spiking activity in the motor cortex appear highly variable across repetitions of an identical task[1]. Hence, any successful biologically realistic model of cortical motor control must provide a mechanistic explanation for both types of variability.

Over the past decades, attractor dynamics has been established as the most viable mathematical concept and computational model to support working memory and decision making in sensory-motor tasks, and there is considerable experimental evidence to support it[2–8]. Yet, despite the fact that the basic theory of attractor dynamics is well understood[9–11], its robust implementation and functional application in biologically realistic spiking neural network models remains a challenge.

The classical cortical model is the balanced network of excitatory and inhibitory neurons with random connectivity[12,13]. This model successfully captures certain aspects of cortical spiking dynamics, including low spontaneous firing rates and irregular spiking statistics. However, it fails to explain the observed cortical trial-to-trial variability and cannot accommodate metastable attractors, which strongly limits its functional capacity. Over recent years, the balanced random network has been extended to accommodate strongly interconnected neuron clusters. With carefully tuned network parameters, this architecture introduces multistable attractor dynamics and can capture aspects of cortical trial-to-trial variability dynamics[14–18]. These studies used purely excitatory neuron clustering but neglected any structure in the topology of local inhibitory networks.

Despite the vital role of inhibitory neurons in cortical dynamics, the circuit connectivity of inhibitory neurons has remained poorly understood until recent years. Several influential studies provided evidence that inhibitory interneurons connect non-specifically to surrounding excitatory pyramidal cells[19,20], which inspired the term 'blanket of inhibition' and supported the rationale behind a purely excitatory cluster topology[14,15]. However, additional studies now provide a more complete picture, suggesting a high degree of speci-

ficity and possible clustering of inhibitory neurons[21–28]. In particular, it has been argued based on anatomical and physiological evidence that inhibitory networks can be strongly interconnected locally. Moreover, neurons that receive strong excitatory input typically also receive strong inhibitory input, supporting local balancing at the level of single cell input[21,29,30]. In addition, recent theoretical studies have corroborated the importance of inhibition in attractor type dynamics and found, based on the analytical treatment of binary and firing rate models, that inhibitory clustering strongly improves the robustness of the metastable dynamics[31].

In the present study, we propose a novel network architecture for spiking cortical attractor networks using combined excitatory and inhibitory clustering. We show that inhibitory clustering maintains the local balance of excitation and inhibition and yields the desired multistability robustly over a wide range of network sizes and parameters. We utilize our model to mechanistically explain task-related dynamics of multiple single-unit activity recorded from the monkey motor cortex during a delayed reaching task. We find that our model qualitatively and quantitatively captures *in vivo* firing rates, task epoch related dynamics of trial-to-trial variability and spiking irregularity, and behavioral reaction times. Variation of the behavioral task involved different levels of target uncertainty during the delay period and resulted in corresponding levels of neural trial-to-trial variability and the systematic variation in behavioral reaction times, both in the monkey data and in our model simulations.

2 Results

Spiking networks with local excitatory-inhibitory clusters can explain cortical variability dynamics in vivo. We start out with analyzing the temporal dynamics of spike train variability in single-unit recordings from the motor cortex of the macaque monkey during a delayed center-out reach task (see Materials and Methods[32,33]). The

monkey was instructed to reach for one of six target buttons at the end of an instructed delay period during which a varying degree of target certainty was cued by either one, two or three adjacent targets. We first consider the simplest task condition in which complete target information was provided to the monkey with the onset of the preparatory period (preparatory signal, PS, indicated by the green circle in Fig. 1a). After a fixed delay of one second the monkey was prompted to execute the movement by the response signal (RS, red circle). Correct execution of a trial was rewarded with fruit juice.

Common statistical measures for quantifying the variability dynamics of spiking neurons are the Fano factor (FF) and the local coefficient of variation of inter-spike intervals (CV_2)[34,35]. The FF determines the neural response variability across the repetition of trials while the CV_2 measures the variability of the inter-spike intervals and thus quantifies the irregularity of spike occurrences within each trial. We apply both measures in a time-resolved fashion using a sliding observation window (see Materials and Methods[35]). Fig. 1a shows that during spontaneous activity and before cue onset (PS) trial-to-trial variability is high (FF ≈ 1.8). After PS, the FF decreases significantly (red curve in Fig. 1a) before reaching a constant plateau. This task-related reduction of the FF has been demonstrated previously in motor cortices and for different behavioral tasks[33,36–38] as well as in other cortical areas[37,39]. The irregularity of inter-spike intervals, CV_2, on the other hand, remains constant over time (black curve in Fig. 1a) and does not show any dependency on the experimental epochs. For the Poisson process the expectation is $FF = CV_2 = 1$ (dashed gray line in Fig. 1a).

Next, we study variability dynamics in a biologically plausible spiking network model of the cortex with excitatory cluster topology. Deviating from the random balanced network, the excitatory neuron population is divided into subpopulations with strong internal connectivity while excitatory connections between clusters are comparatively weak[14–17]. The model is composed of 4000 excitatory (E) and 1000 inhibitory (I) exponential integrate-and-fire neurons. The E neurons are organized into $Q = 50$ recurrent clusters (Fig. 1b top

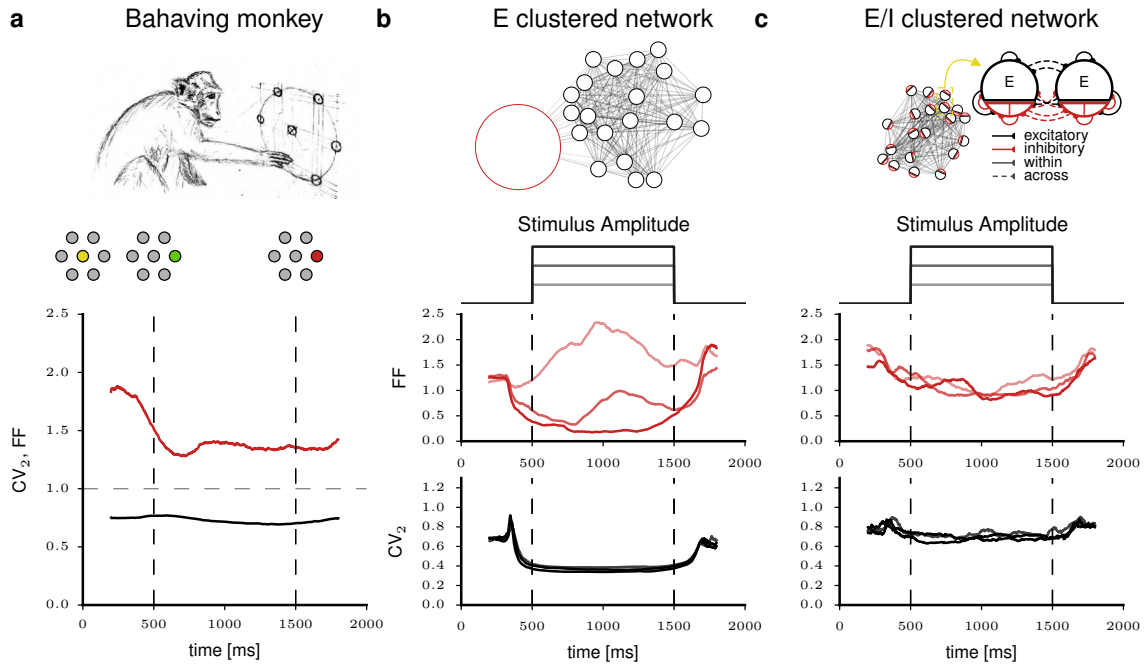

Figure 1: **Variability dynamics observed experimentally and in clustered spiking network models. a)** Experimental data recorded from the motor cortex of a macaque monkey during a delayed center-out reach task[33]. Time-resolved Fano factor (FF) and coefficient of variation (CV_2) averaged across neurons are shown in red and black, respectively. Gray horizontal dashed line shows FF and CV_2 for the Poisson process. Vertical dashed lines indicate PS (when green target LED was lit) and RS (when red target LED was lit). **b)** Network model with purely excitatory clusters and global inhibition (E clustered network). The amplitude of the step-wise external input is shown in shades of gray, the corresponding time-resolved FF is shown in shades of red and the time-resolved CV_2 in shades of gray; the lighter the color, the weaker the stimulus amplitude. **c)** Same analyses as in (b) but for the proposed network model with excitatory and inhibitory clusters (E/I clustered network). FF and CV_2 were computed in a 400 ms sliding window; simulated data comprised 50 trials.

panel). Synaptic connections within each cluster are potentiated by a factor J_+, and to maintain overall balance, connections between E neurons belonging to different clusters are depressed by a factor J_-. Inhibitory neurons are non-specifically connected to themselves and to E neurons (see Materials and Methods).

We simulate 2000 ms of network activity. After 500 ms of spontaneous activity, $\sim 10\%$ of the clusters were stimulated during 1000 ms. We again quantified variability dynamics of FF and CV_2 in a sliding window. Fig. 1b shows the temporal modulation of FF for different stimulus amplitudes. A consistent reduction in FF upon stimulation can only be achieved with a strong stimulus (dark red curve) whereas the E-clustered network can show inconsistent behavior or even an increase in FF for stimuli of intermediate or low strength (light red curve), inconsistent with our experimental observations. As for the regularity dynamics, we observe a reduction in CV_2 during stimulation that tends to be stronger for a stronger stimulation. This stimulus-induced increase in regularity is again clearly inconsistent with our experimental observations (see Fig. 1a) and, to our knowledge, has not been reported in any other study. In summary, the E-clustered network is inconsistent with the experimental observations in two ways: (1) a reduction in count variability (FF) is achieved only with a strong stimulus, while a weak stimulus can lead to an increase in FF; (2) during network stimulation the irregular spiking is disrupted, and the CV_2 assumes unrealistically low values.

To match the experimentally observed stimulus-induced variability dynamics, we suggest a novel type of network connectivity. Recent anatomical and physiological studies point to a high local connectivity and a possible clustering of inhibitory neurons[21–23,25–28]. We therefore combine excitatory and inhibitory clustering in our spiking network model following our previous proposal for binary networks[31] (Fig. 1c top panel). We simulate this E/I-clustered network model using the same parameters as for the E-clustered network (Materials and Methods). Fig. 1c shows that the trial-to-trial variability (FF) decreases robustly even for a weak network stimulation while the CV_2 does not show any stimulus-

induced changes, matching our experimental observations (Fig. 1a). We will next investigate the network mechanisms that support realistic variability dynamics in E/I-clustered but not in E-clustered networks.

Metastability emerges robustly in the E/I-clustered spiking network. We first ask which network parameters determine the emergence of metastability and winnerless competition among embedded clusters. To answer this question we examined the effect of two important clustering parameters, the clustering strength J_+ and the number of clusters Q for a fixed network size. Metastability is expressed in the successive activation and inactivation of individual neuron clusters where individual neurons switch between lower and higher firing rate states. Across repeated observations of individual neurons we therefore expect a high variation of the spike count; thus, the FF provides a proxy for metastability.

We again consider a network of 4000 excitatory and 1000 inhibitory neurons (Table 1). We first kept the number of clusters $Q = 50$ fixed and varied the cluster strength between $J_{E+} = 1$, which coincides with the classical random balanced network without clustering, to $J_{E+} = Q = 50$ with zero excitatory coupling between different clusters (see Material and Methods). The E-clustered network (Fig. 2a) can show metastability as indicated by the alternating firing rate states of individual cluster populations (insets in Fig. 2a) only in a very narrow range of excitatory cluster strengths around $J_{E+} \approx 3.5$, which is accompanied by correspondingly large Fano factors (FF > 1). When increasing J_{E+}, the cluster dynamics rapidly breaks down and the FF falls below its initial value associated with the random balanced network ($J_{E+} = 1$) and eventually the network gets stuck in a single state with a few clusters becoming permanently active with high firing rates and regular spiking patterns.

A different picture emerges in the E/I-clustered network (Fig. 2c). Metastability is achieved over a wide range of J_{E+}. With increasing cluster strength, the duration of

individual cluster activations becomes longer. For large values $J_{E+} \gtrsim 15$ the variance over repeated simulations is high, as some cases exhibit extensive cycling between clusters while in other cases one or a few clusters become dominantly active and suppress the winnerless competition dynamics. At $J_{E+} = Q = 50$ coupling between the populations exists only through strong inhibitory connections and most populations are silenced by a few winning clusters. The desired attractor dynamics thus takes place at lower values of J_{E+}, which yield realistic average trial-to-trial variability in the approximate range $1 < \mathrm{FF} < 3$.

In a next step we in addition varied the number of clusters Q while keeping the total number of neurons N fixed. This changes the size of each cluster, i.e. larger Q means a smaller number of neurons per cluster. For the purely excitatory cluster topology (Fig. 2b) we find that there is only a very small parameter region that shows high spike count variability across repeated observations ($\mathrm{FF} > 1$). Thus, the E-clustered network is able to facilitate winnerless competition, but stable switching dynamics can be achieved only by extensive parameter tuning. In contrast, in the E/I-clustered network attractor dynamics as indicated by high $\mathrm{FF} > 1$ emerges robustly over a large range of cluster numbers Q and excitatory cluster strengths J_{E+} as shown in Fig. 2d. This means that metastability in the E/I-clustered network is not sensitive to variations or perturbations in network parameters. Importantly, the E/I cluster topology supports metastability even for large networks in contrast to the E-clustered network where attractor dynamics breaks down for larger network sizes.

Local balance of excitation and inhibition facilitates attractor dynamics and maintains spiking irregularity. Synaptic excitation and inhibition are opposing effects that together determine the activity and maintain the excitability of cortical neurons and networks[29,40,41]. A number of physiological studies have shown that excitatory and inhibitory synaptic inputs retain a fixed and roughly equal proportion during both spontaneous and evoked states[30,42–46]. This mechanism known as balance of excitation

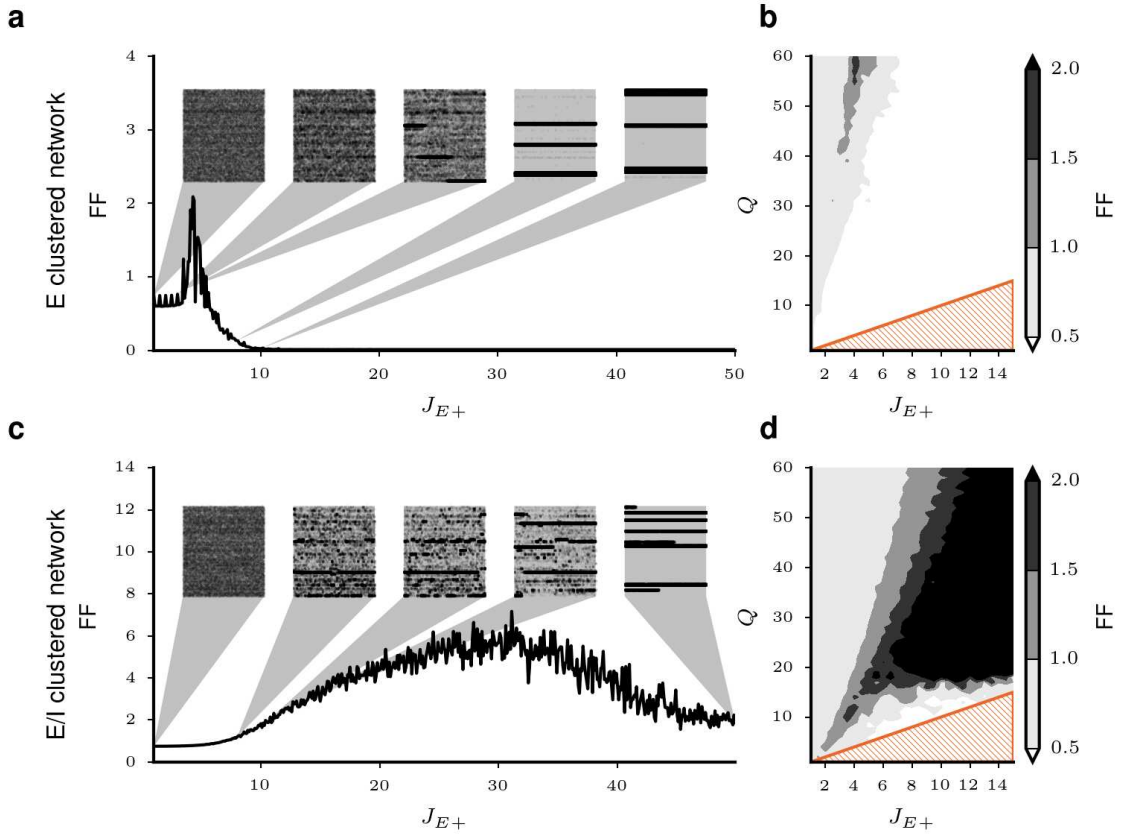

Figure 2: **Excitatory-inhibitory clustering facilitates winnerless competition across a wide range of network parameters. a, c)** FF versus J_{E+} for networks with $Q = 50$ clusters computed from 20 trials of 400 ms duration and averaged over 50 network realizations. Insets show two seconds of single trial network activity for all excitatory neurons grouped by their cluster identity. **b, d)** Effect of cluster strength J_{E+} and number of clusters Q on metastability and trial-to-trial variability (FF). Shaded orange triangles indicate the zone below $J_{E+} = Q$, where the clusters are completely decoupled. Panels **a, b** show results for the E-clustered network; **c, d** for the E/I-clustered network. Parameters apart from J_{E+} and Q as in Table 1.

and inhibition is crucial for maintaining irregular spiking and stable network activity, and disruption of this balance has been linked to pathological activity states such as epileptic seizures.

In this section we study the balance of excitation and inhibition in E and E/I-clustered networks. Using again the parameters in Table 1 we simulate 1000 ms of spontaneous activity of E and E/I-clustered networks with $Q = 50$ clusters. Fig. 3 illustrates the difference between E-clustered (left panels) and E/I-clustered (right panels) networks on the level of individual neurons. The raster plot in Fig. 3a shows the activity of nine sample excitatory clusters in the E-clustered network. Neurons across all nine clusters exhibit low firing rates until at about t = 350 ms one cluster switches into an activated state. The corresponding instantaneous firing rate averaged across all neurons in the activated cluster increases strongly to almost 90 spikes/s, whereas the firing rates of the other clusters remain low. Fig. 3e shows the synaptic input currents to one single neuron in the activated cluster around the switching time (red shaded interval in Fig. 3a). While the excitatory input current increases (I_E, upper trace) due to the strong mutual excitation within this cluster, the inhibitory input (I_I, lower trace) remains constant. As a result, the net input current (I_{tot}, middle trace) increases to positive values and hence the neuron operates in the mean-driven rather than in the fluctuation-driven regime. As a result, a large portion of the neurons in the active cluster fire with high rates and high regularity, as can be seen in the membrane potential of the example neuron depicted in Fig. 3g. This provides the mechanistic explanation for our results of a strongly decreased CV_2 in Fig. 1b.

The right-hand side of Fig. 3 analyzes the equivalent scenario for an E/I-clustered network. The raster plot in Fig. 3b indicates that in this spontaneous state individual clusters can switch from an inactive state with low ongoing firing rates to activated states of variable duration. This attractor dynamics involves moderate firing rates during activated states (Fig. 3d), which are considerably lower than the high firing rates observed in the E-clustered network Fig. 3d. The synaptic input currents in a sample neuron are shown in

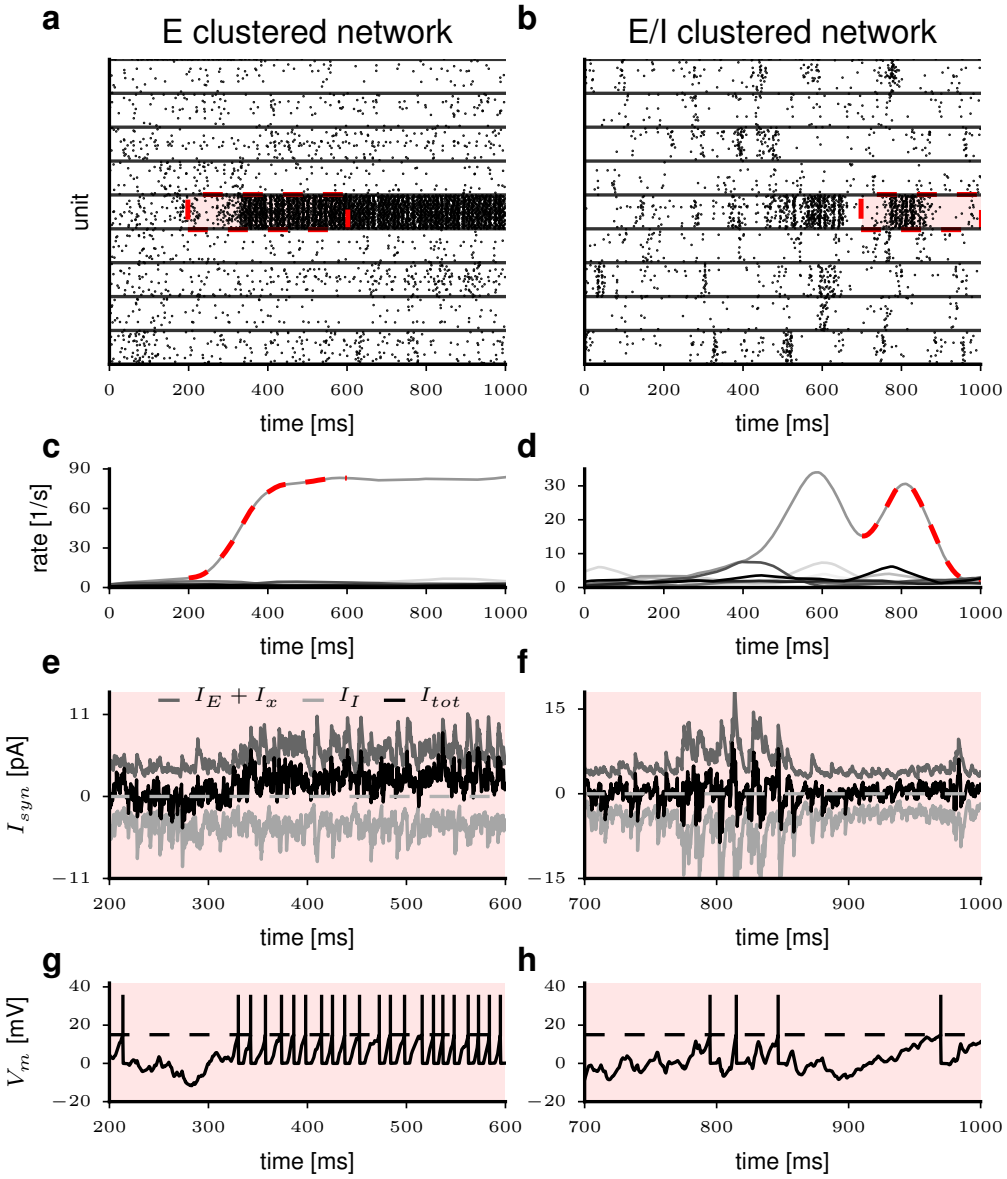

Figure 3: **E/I clustering maintains local balance of excitation and inhibition and irregular spiking.** Comparison of E-clustered (left) and E/I-clustered (right) networks. **a, b)** Spike raster display of nine excitatory clusters during 1000 ms of spontaneous activity. Horizontal lines separate different clusters. Red shaded area indicates the epoch of interest where a switch into an active state occurred in one cluster. **c, d)** Average firing rate of each of the nine clusters shown above as estimated with a 50 ms triangular kernel[47]. Dashed lines correspond to the red shaded region of interest in the upper panels. **e, f)** Synaptic currents in a randomly chosen unit around the switch to the active state within the cluster and epoch of interest indicated above. **g, h)** Membrane potential for the unit shown above in the same time interval.

Fig. 3f, again at the transition from the inactivated to the activated state of its cluster. In effect, inhibitory clustering ensures that the inhibitory synaptic currents increase in parallel with the excitatory synaptic currents during cluster activation, thereby increasing the variance but not the mean of the net synaptic input, which is kept balanced throughout. Hence, all neurons remain in the fluctuation-driven regime and retain irregular spiking as illustrated in Fig. 3h and shown for the network population in Fig. 1c.

E/I clustering linearizes stimulus-response function and increases response range. We have seen that the E-clustered network fails to capture the reduction in trial-to-trial variability during stimulation with a weak stimulus (Fig. 1). Here we ask what exactly constitutes a weak stimulus by analyzing in detail how the cluster response rate and the change in trial-to-trial variability depend on the stimulus amplitude in networks with and without inhibitory clustering. To this end we stimulated five out of 50 clusters by means of a constant input current injected into all neurons belonging to these clusters (Fig. 4a). In our analysis we compare network activity in the spontaneous state (before stimulation) with the network activity during the evoked state (during stimulation) and calculate the changes in firing rate (Δrate) and FF (ΔFF) as a function of stimulus strength. Fig. 4b shows the average Δrate separately averaged across all neurons in the stimulated or non-stimulated clusters as a function of stimulus amplitude, resembling a population-averaged I-F curve. In the stimulated clusters of the E/I network we observe an approximately linear relation between input current and firing rate increase in the tested stimulus range. In the case of a purely excitatory cluster topology the firing rate in stimulated clusters increases steeply with increasing current amplitude and this relation shows a negative acceleration. The non-stimulated clusters exhibit a small decrease in their average firing rate during stimulation.

The dynamics of trial-to-trial variability shows a clear difference in the two different network topologies. In the E-clustered network, there is a stark increase in FF for stimulus

amplitudes in the lower half of the stimulus range of up to $\sim 0.4\,\mathrm{pA}$ (Fig. 4c). The desired effect of a reduced FF is achieved only for increasingly large input currents that correspond with high cluster rate responses of $\Delta\text{rate} > 40$ spikes/s (cf. vertical dashed line in Fig. 4b and c). This means that the E-clustered network fails to reproduce the experimentally observed reduction in trial-to-trial variability for weak stimuli and moderate average neuronal response rates. The reason for the increase in variability for weak to moderate stimulus amplitudes is that stimulated clusters switch into an activated state in some trials but fail to do so in others (not shown), i.e. cluster activation is unreliable. This coincides with our theoretical prediction based on the analytic treatment and numerical simulation of binary cluster networks where stable fixed points require considerable excitatory input stimulation and can assume only high cluster rates (Rost et al.[31]).

In contrast, the E/I topology shows a reduction in trial-to-trial variability of single-neuron spiking in stimulated and non-stimulated clusters even for weak stimuli of $\gtrapprox 0.1\,\mathrm{pA}$ (Fig. 4d) and correspondingly low average cluster response rates (Fig. 4b). This reflects that clustering stimulation reliably initiates switching into an excited state in each single trial. The range of ΔFF in the models closely matches the average ΔFF observed in the experimental data (cf. Fig. 1a).

In summary, the E/I-clustered network robustly captures the reduction in trial-to-trial variability during stimulation and retains a linear relationship between stimulus strength and rate response, while the E-clustered network fails to reproduce the reduction in trial-to-trial variability for weak stimuli and low to moderate population rates.

Motor cortical activity reflects target uncertainty during movement preparation and execution. We now analyze the monkey's behavior and motor cortical single-unit activity during the delayed reach task in its full complexity. As shown in Fig. 5 a the monkey performed the task under three different conditions that varied in the amount of cued target information. At the beginning of the 1 s delay period and in

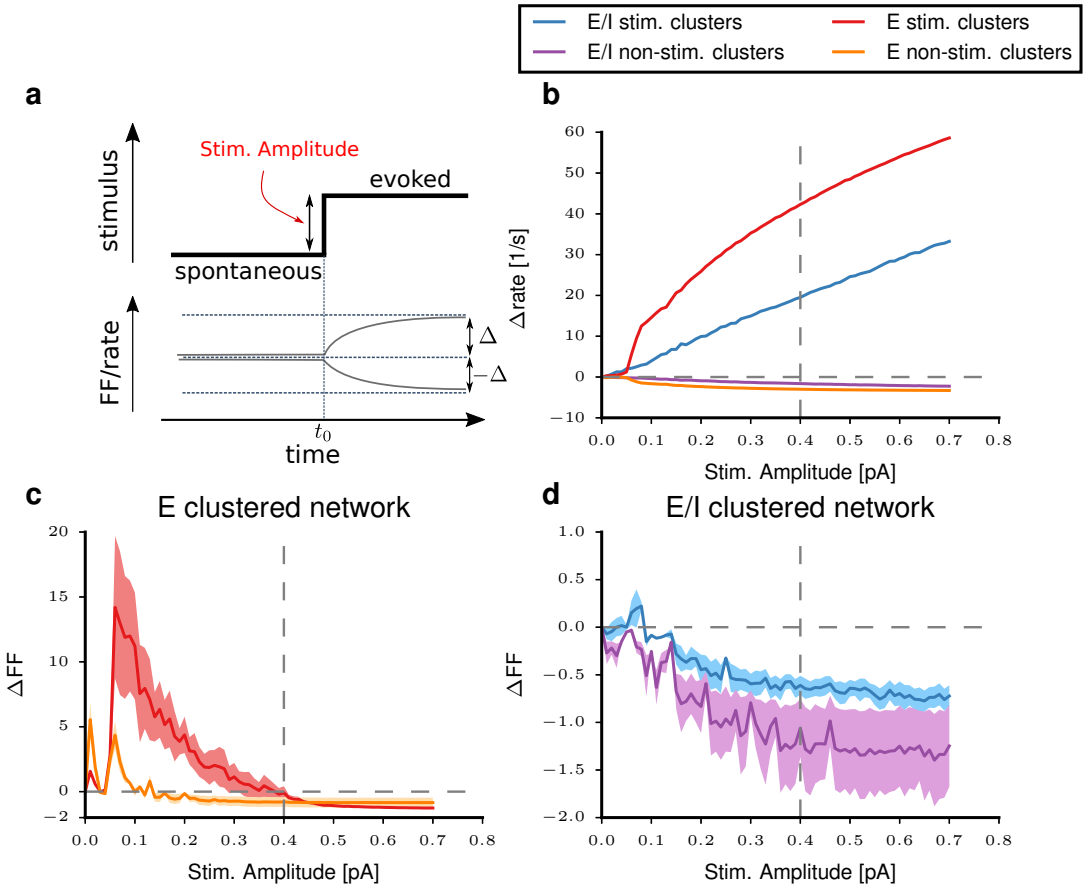

Figure 4: **Stimulus-evoked changes in firing rate and trial-to-trial variability. a)** Cartoon depicting the stimulus-induced transition from the spontaneous to the evoked cluster state. Upper panel shows the step change in the external input current at time t_0. Lower panel depicts the stimulus-induced changes in the average firing rate or FF relative to the spontaneous level. Stimulation is applied to 5 out of the total of $Q = 50$ clusters, leaving 45 non-stimulated clusters. **b)** Average stimulus-response function Δrate versus the amplitude of the injected step current. Different colors indicate the behaviors for stimulated and non-stimulated clusters in the E and E/I-clustered networks as indicated in the legend. **c,d)** ΔFF versus stimulus amplitude for the E-clustered network (c) and the E/I-clustered network (d) estimated across 50 trials. Both measures are calculated for 1000 ms of spontaneous and evoked activity, respectively. The difference is computed for each neuron separately before averaging across neurons. Firing rate differences of single units were averaged across the 50 trial repetitions. Shaded areas show the standard error of the mean calculated across the stimulated and non-stimulated clusters, respectively. Network parameters as in Table 1.

Condition 1, the PS cued a single target by a green light (full target certainty). The target light turned red at the end of the delay period (RS), prompting the monkey to move. In Condition 2, the PS cued two possible targets by two adjacent green lights, one of which was then randomly chosen as the final movement target (single red light) presented as RS. Condition 3 implied the highest target uncertainty during the preparatory period with three possible adjacent targets cued by the PS.

We first analyzed the encoding of movement direction in the motor cortical single-unit activity. To this end, and reconsidering the approach taken in Rickert et al.[33], we trained and cross-validated a classifier to predict the direction of the executed movement in each trial based on the neuronal population activity (see Material and Methods). We then computed the decoding accuracy, i.e. the fraction of correctly predicted single-trial movement directions, as a function of trial time as shown in Fig. 5b. In all three task conditions and during the preparatory period the decoding accuracy reaches the theoretical limit that reflects the target information available to the monkey. When full information was available (Condition 1), decoding accuracy approaches unity. When target information was incomplete with either two or three possible targets indicated at PS, the decoding accuracy levels at $1/2$ and $1/3$, respectively, accurately reflecting target uncertainty. After the RS resolved target ambiguity by indicating the final single movement target, decoding accuracy approached unity in all three conditions.

Next, we asked whether task uncertainty modulates trial-to-trial variability of the single-unit activity. We therefore computed ΔFF as a function of trial time comparing the result across the three different task conditions in Fig. 5c. In all three conditions, spike count variability is initially quenched in reaction to the PS. Subsequently, the FF recovers to a different level depending on the condition. In the case of complete target information (Condition 1) the FF remains at a low value, while in Condition 2 it resumes a higher, and in Condition 3 a still higher plateau value. The differences between the task conditions are statistically significant. Thus, the level of trial-to-trial variability of

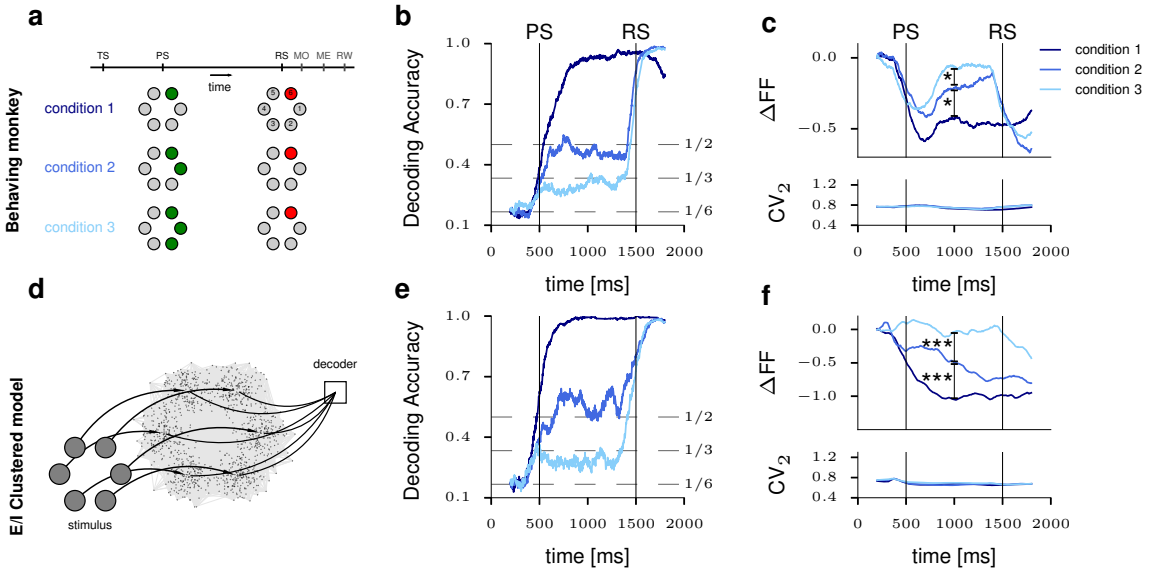

Figure 5: **Functional E/I-clustered model captures context dependency of information encoding and variability dynamics. a)** Experimental protocol of the delayed center-out reach task: 500 ms after trial start (TS) the preparatory signal (PS) indicated either one, two or three adjacent targets in green, corresponding to Condition 1 (full target information) and Conditions 2 and 3 (incomplete target information). After a fixed delay period of 1000 ms the preparatory signal (PS) resolved target ambiguity by indicating the final movement target in red, prompting the monkey to execute the movement. The movement onset time (MO) and movement end time (ME) are recorded in each single trial. **b)** Accuracy of decoding movement direction from the neuronal population activity for the three task conditions. **c)** Upper panel: Task-related reduction in trial-to-trial variability ΔFF as a function of trial time; $*$ indicates pairwise significant differences across FF distributions (Wilcoxon signed rank test, Conditions 1-2: $p = 0.007$, Conditions 2-3: $p = 0.03$). Lower panel: Time-resolved estimate of the CV_2. **d)** Architecture of the E/I-clustered attractor network model. Each of the six embedded clusters represents one target direction and can receive excitatory input with the PS and RS stimuli. Each cluster is assigned a direction for which it receives its external input. The decoder integrates the average cluster firing rates and generates a decision. **e, f)** Analysis as in b-c but for neurons in the spiking network model. Distributions of FF are significantly different as determined by a Wilcoxon signed rank test (Conditions 1-2: $p = 3.6 \times 10^{-13}$, Conditions 2-3: $p = 3.7 \times 10^{-30}$). Decoding accuracy, FF and CV_2 were estimated in a sliding window of 400 ms width.

single-neuron spiking activity directly reflects target ambiguity during the preparatory period, where less/more uncertainty implies less/more variability. Following the RS and during movement execution, the FF shows an additional reduction in Conditions 2 and 3. No additional reduction in FF is visible in the single-target condition. Note that the average single-neuron spiking irregularity (CV_2) in Fig. 5c (lower panel) remained constant throughout the task and in all three conditions at a value of $CV_2 \approx 0.8$.

Motor cortex model provides mechanistic explanation for task-dependent movement encoding and variability dynamics. We now examine whether and how an attractor-based model of the motor cortex can reproduce our experimental observations in the behaving monkey. To this end we propose a functional spiking neural network model that combines the E/I cluster topology with an additional decoder module to support behavioral decision making as schematically shown in Fig. 5d. The core of this model consists of six E/I clusters, one for each target direction. In our simulations we mimicked the behavioral monkey experiment by applying the same stimulus protocol. Starting with the onset of the PS (Fig. 5a) we stimulate all neurons of either one, two or three clusters representing the visual cue presenting either one, two or three adjacent targets throughout the preparatory period. The amplitude of the stimulation current was identical for all clusters. With the RS, i.e. at the end of the preparatory period, stimulation was maintained for only a single cluster that represented the final target. In a continuous simulation the model was faced with 150 trials in each of the three stimulus conditions.

We subsequently repeated the exact same analyses of directional encoding and of variability dynamics on the spike train recordings during model simulation (Fig. 5e–f) as for the experimental *in vivo* recordings. The classification analyses, now applied to the entire population of excitatory model neurons, resulted in average decoding accuracies that fully resemble those observed in the experimental data (compare Fig. 5b and e), recovering the optimal decoding scores of 1, 1/2 and 1/3 that reflect the respective target

uncertainty in Conditions 1, 2 and 3. This can be explained by the probabilistic nature of a switching activation between the stimulated clusters. As an example, Fig. 6a shows the spiking activity of all excitatory neurons in the model during a sample trial of Condition 3. With the onset of the PS a stimulus current was applied to clusters 1, 3 and 4 (counting from the bottom). After cue onset, competition arises between these three clusters. All three clusters now *share* the same higher probability of being active as compared to the non-stimulated clusters. On average the activation times for all three clusters are thus equal and therefore represent the randomly selected final target with probability 1/3 at each point in time. After RS, only the neurons in cluster 3 that represents the selected final target receive stimulating current input and becomes active.

The time-resolved variability analysis of the model data captures the condition-dependent temporal modulation of the average ΔFF observed *in vivo* (compare Fig. 5c and f) where the reduction in FF is largest for the single target cue and smallest for the triple target cue. The average spike time irregularity (CV_2) of the model neurons is essentially constant throughout the trial and independent of the target condition, in full agreement with our experimental results. The reflection of target uncertainty in the trial-to-trial variability during the preparatory period is mechanistically explained by our model. Stimulation of a single cluster (Condition 1) makes it very likely that this E/I cluster becomes activated, while all other clusters are likely to stay inactive for most of the 1s preparatory period. Across repeated trials of the same single target cue, neurons of the same stimulated cluster exhibit elevated firing rates while all other neurons are likely to show a low firing rate. Hence, the across-trial variability of the spike count is low. When there is competition between two or three stimulated clusters, the neurons of these clusters share the overall activation time and hence the FF will be higher.

A simple model of decision making operating on cluster population activities can explain modulation of behavioral reaction times. Inspired by previous models

of perceptual decision making[48,49], the decoder module in Fig. 5d generates a decision variable associated with each cluster. For each target direction d, a leaky integrator governed by an equation of the form

$$\frac{dI_d(t)}{dt} = -\frac{I_d(t)}{\tau_I} + C_d \tag{1}$$

integrates the instantaneous spike count of the corresponding neuron population and forgets with time constant τ_I. The decision variable $DV_d(t)$ is formed as

$$DV_d(t) = \frac{I_d(t)}{\sum_{j=1}^{6} I_j(t)} \tag{2}$$

expressing the probability that target direction d represents the correct choice of movement direction at time t. This is similar to multi-class classification. A behavioral decision was reached when one of the decision variables crossed the common threshold θ within a 400 ms interval following the RS. Threshold crossings after that period were counted as unsuccessful trials. This is similar to the monkey experiments where the monkey had to react within a short time limit. If a decision variable was already above threshold at the beginning of the response signal (RS), the decision was counted. The threshold was adjusted such that the average accuracy over all sessions is maximized.

The operation of the decoder is illustrated in Fig. 6a where the respective decision variables $DV_d(t)$ are superimposed on the neural population activity of each target cluster. In this example trial of Condition 3, the clusters 1, 3 and 4 receive stimulation during the preparatory period while target cluster 3 was randomly chosen as the final target indicated by the RS. At the time of RS onset, cluster 1 is still activated and it takes a short time until the change in stimulus takes effect and a switch occurs that finally activates cluster 3. Subsequently $DV_3(t)$ increases and reaches the threshold after a model reaction time of ~ 400 ms.

Fig. 6b-c show the distributions of reaction times produced by the model and experi-

mental data, respectively, for each condition. It can be seen that as in the experimental data the average reaction times in Condition 1 were much shorter than in Conditions 2 and 3. In contrast to the experiment, anticipated responses were not penalized in the model. If the decision variable of the correct direction was already above threshold at RS, the trial was counted as successful. In Condition 1 this was frequently the case. The shape of the reaction time histogram for Condition 1 (dark blue in Fig. 6c) suggests that the monkey displayed a similar behavior. Both the data and the model show on average slightly larger response times in Condition 3 compared to Condition 2. The possibility of having *prepared* for the wrong direction in the model explains the difference in reaction times between the full information and the ambiguous conditions.

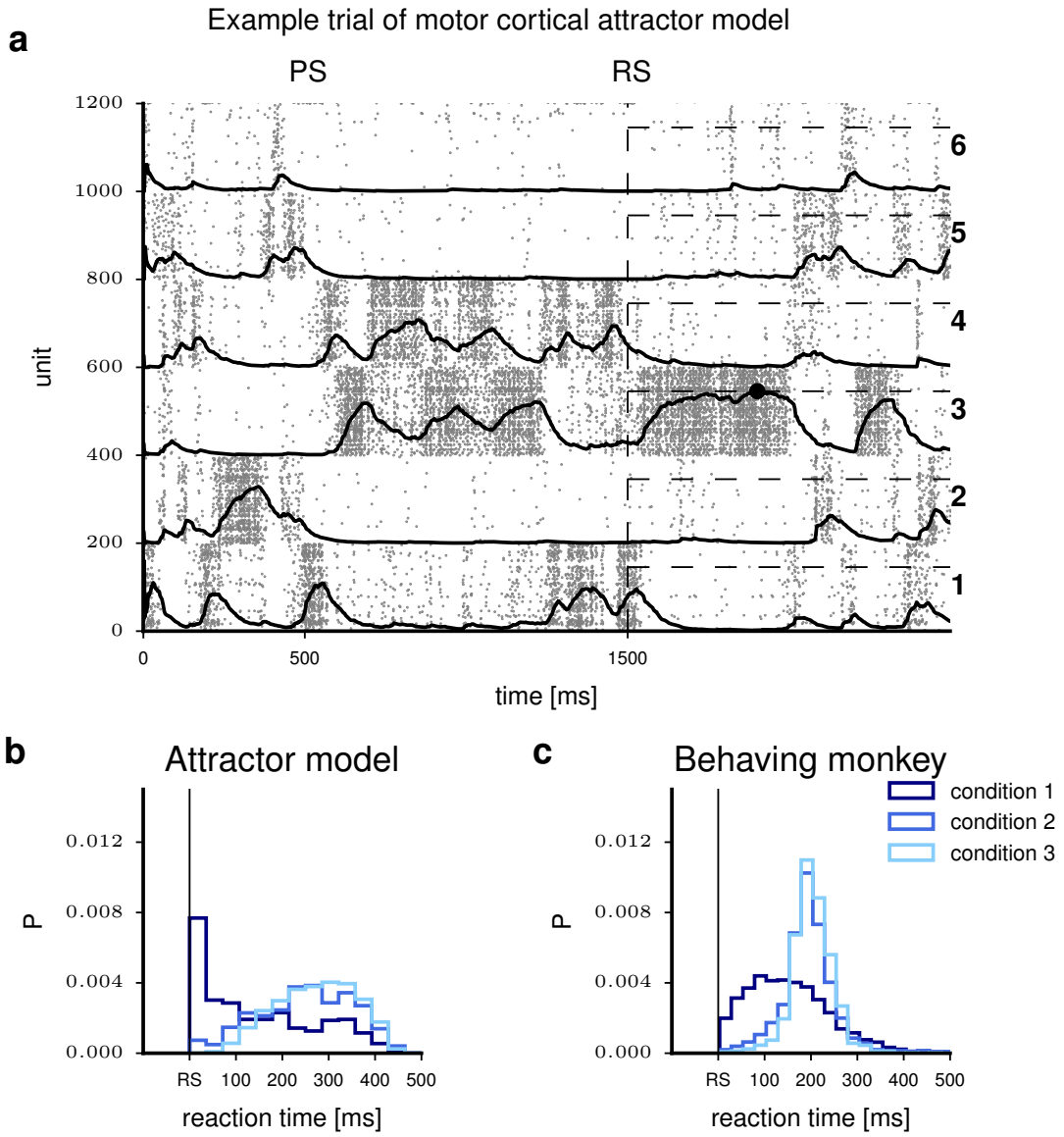

Figure 6: **Decision model generates task-dependent reaction times. a**) Raster plot of excitatory cluster activity for an example trial of Condition 3. Solid curves represent the decision variable (DV; equation 2) associated with each cluster. At $t = 1500$ ms the decoder starts integrating, as indicated by the vertical dashed line. Horizontal dashed lines show the level of the decision threshold θ. To the right, target direction numbers are indicated. During the preparatory period (between PS and RS), clusters 1, 3 and 4 are stimulated. The final target (direction 3) was randomly chosen, resulting in a continued stimulation of only cluster 3 after RS. The black circle indicates the decision for a movement in direction 3 by means of threshold crossing. **b-c**) Histograms of *reaction times* of the model (b) and the experimental data (c) for all three task conditions.

3 Discussion

We have proposed a robust mechanistic model of cortical and behavioral variability dynamics and showed that it accounts for task-related dynamics and coding in motor cortex. The model extends previous spiking attractor network models featuring excitatory clustering[10,14–18] by adding clustered inhibitory connectivity, motivated by recent experimental[21,22,24,25,27,28] and theoretical[28,31] studies. We showed that the clustered inhibition ensures the local balance of excitation and inhibition within each attractor, and increases the robustness of winnerless competition, able to capture cortical dynamics during decision-making. The model replicates both neural and behavioral variability of a monkey performing a delayed reaching task with various degrees of prior information about the target direction. At the neuronal level, we showed that our model reproduces the spiking irregularity and trial-to-trial variability of spike counts, and at the behavioral level, our model captures the reaction times during the task. These findings suggest joint excitatory and inhibitory clustering as a powerful mechanism for decision-related activity in cortex.

Joint excitatory and inhibitory clustering vs. purely excitatory clustering Previous studies have considered purely excitatory clustering with a 'blanket of inhibition' to explain decision-related activity in cortex and the associated cortical variability dynamics[10,14–17]. We here showed that joint excitatory and inhibitory clustering better accounts for cortical variability dynamics, thereby more plausibly reflecting the neural mechanisms underlying decision-making. Furthermore, recent evidence in the literature supports the notion that not only excitatory neurons but also inhibitory neurons in cortex are clustered[21–28].

Cortical neuronal activity is variable on both the single-trial level, in terms of the irregularity of interspike intervals, and across trials, measured for instance by the Fano factor. Our experimental data show that spike timing irregularity is comparable during

spontaneous and evoked activity, while trial-to-trial variability is lower for evoked activity. Switching between clusters in a process of winnerless competition is able to account for the high Fano factor during spontaneous activity, while the variability is quenched during evoked, decision-related activity by selection of a single cluster or subset of clusters.

Spiking attractor network models with clustering only among excitatory neurons have been successful in explaining the trial-to-trial variability observed in *in vivo* recordings. However, this type of model has unrealistic spiking irregularity and excessive spike rates during cluster activation and exhibits biologically plausible multistability (winnerless competition) only in a narrow parameter regime (see Fig. 2 and discussion of Litwin-Kumar et al.[14], Deco et al.[15] and Rost et al.[31]).

By analyzing the stable fixed points of the mean-field equations for networks with excitatory clusters, Rost et al.[31] have shown that switching is hampered by the high rates attained in active clusters. Our proposed remedy of assigning an inhibitory population to each cluster, by increasing the corresponding E $\rightarrow$ I, I $\rightarrow$ E and I $\rightarrow$ I synaptic strengths, solves both of the above problems. Since inhibition is now also selective, each excitatory population is held in check by its inhibitory counterpart and hence the fixed points of the active and passive clusters move closer together. This facilitates switching, and also helps to maintain interval variability because the active clusters remain in the fluctuation-driven balanced state rather than being forced into saturation (see Fig. 3). Thus, inhibitory clustering ensures realistic spike timing variability and greatly increases the robustness of the multistability, extending the range of cluster strengths and sizes over which winnerless competition occurs.

Functional role The balanced random network model with joint excitatory and inhibitory clustering not only accounts for realistic cortical variability dynamics but also reproduces functional and behavioral aspects of movement preparation and decision-making: task-related encoding, variability, and reaction times match the experimental observations.

In our experiment when the monkey has incomplete information during the preparatory period it can only resolve the ambiguity of multiple targets when the RS signal provides full information, and the reaction times are increased. We observe the same phenomenon in our model. The mechanistic explanation is that in the multiple-target conditions the clusters compete and the activity switches between them during the preparation period. When the RS signal resolves the ambiguity, only one of the clusters retains input stimulation. If this cluster has been active at this point in time, the activity level reaches the threshold faster (short reaction times) than in the case where a switch is required, leading to longer reaction times (Fig. 6). The same mechanistic explanation underlies short and long reaction times in a recent attractor network model describing behavioral reaction times in anticipatory versus unexpected cues depending on pre-stimulus cluster activation[17]. In our model we find a small but non-negligible increase in reaction times from the two-target to the three-target condition. The same effect was observed in the monkey's reaction time. Our model mechanistically explains this effect by the lower chance for the cluster associated with the final goal to be active at the time of the RS signal in the three-target compared to the two-target condition.

Multistability and timescales of variability dynamics The timescales on which neural activity varies constitute a recurring theme in the context of cortical variability. The present work is centered around the hypothesis that rate variance across trials is a consequence of slow switching between clusters of neurons. In our model, we have observed that switching tends to occur less frequently when the clustering is stronger, thereby increasing the time that assemblies spend in the active state. A number of physiological results support the hypothesis that spontaneous activity is made up of sequences of structured activity patterns that emerge seemingly at random. The average or typical amount of time spent in each pattern is still a matter of investigation[16,50–53].

These results point to timescales on the order of tens to hundreds of milliseconds. Teich

et al.[54] on the other hand have found that Fano factors of retinal ganglion cells in cats increase with counting window width for observation intervals of several minutes. For stationary point processes, the FF depends only weakly on window size[35]. When rate variance is added to the equation, the Fano factor will increase with counting window size until the window spans several periods of the periodicity of the underlying fluctuations. Such long-timescale fluctuations do not necessarily have to originate from the cluster switching mechanisms described here. It is likely that winnerless competition dynamics in spontaneous cortical firing will happen on timescales related to the stimulus modalities or movements a particular region codes for.

The timescales of switching in our model depend on the value of the cluster parameter J_{E+}. We have adjusted this parameter so that the networks' spontaneous activities exhibit Fano factors similar to those observed in our experimental data. We have not measured the durations that attractors spend in the active states, although an hidden Markov model analysis similar to those by Ponce-Alvarez et al.[52] and Mazzucato et al.[16] could yield estimates. Inspection of the raster plots does however suggest that the up states in our model have similar timescales to those reported in the literature ($\sim 20 - 200\,\mathrm{ms}$).

It would be desirable to have a theoretical prediction for the timescales of cluster switching in relation to the model parameters. Lagzi et al.[55] have described the winnerless competition between two populations using a rate model governed by Lotka-Volterra-type equations. If noise is introduced, switching can also occur in rate models. They found that the survival times of the active states could be well approximated by an exponential distribution and that the average time between switches grows faster than exponentially with cluster strength. Rost et al.[31] used the mean-field description of our network configuration for binary neurons to find the stable rate configurations. Switching between these stable attractors is a finite size effect due to chaotic fluctuations in the firing of individual units in the populations which is by definition not captured by the mean-field approach. The mean-field theory for networks of binary units also predicts the

distribution of activity rates within populations[12]. From this, it is theoretically possible to compute the 2Q-dimensional joint distribution of cluster rates. Under certain assumptions about the noise caused by the rate fluctuations within clusters it may then be possible to make predictions about the switching dynamics. This analysis is, however, beyond the scope of the current study.

Outlook In our study, we varied cluster size and found more robust winnerless competition for smaller clusters, below about 200 neurons per cluster. Switching of activity states is triggered by fluctuations in cluster firing rate. Hence the probability of switching decreases when clusters become larger, because fluctuations tend to average out[56]. While fine-scale clusters have been reported to consist of tens rather than thousands of neurons[57], it is unclear whether the cortical algorithm in reality already breaks down with clusters of a few hundred units. Future investigations into this issue can include anatomical and physiological estimates of cluster size, as well as computational modeling attempting to increase the robustness of winnerless competition for large clusters.

Our experimental data is recorded after an extensive training period so that the monkey performs the task with a high proportion of correct trials. We therefore assume in our model that the connectivity has reached a fixed structure and is no longer plastic. Future work may investigate how the clustered connectivity is learned during training, for instance through spike-timing-dependent plasticity (STDP) combined with selective stimulation[58–63]. To form and recall these clusters in a stable manner over a long time some form of homeostatic mechanism is crucial. Zenke et al.[60] shows that multiple timescales of homeostatic regulation are necessary to form robust and stable clusters that are functionally relevant. Liwin-Kumar et al.[61] investigate homeostatic mechanisms that act on I→E synapses together with E→E STDP rules to form clusters that reflect previously experienced stimuli. The inhibitory plasticity in these studies is globally modulated while excitatory neurons form local clusters and are responsible for functional representations. It

will be interesting to investigate how joint excitatory and inhibitory clustering can stably emerge in neural networks through plasticity, and what role is played by homeostatic mechanisms in this context.

4 Materials and Methods

Experiment

Behavioral task and recordings in the monkey. The monkey experiments were conducted in Alexa Riehle's lab at the CNRS Marseille, France. The monkey performed a delayed center-out reaching task which involved three different task conditions that differed in the amount of initial target information available to the monkey as illustrated in Fig. 5 a. The monkey was seated in front of a panel featuring a hexagonal array of touch-sensitive target LEDs and a central LED indicating the starting position. The monkey initiated a trial by touching the central LED (trial start, TS). During the 1s delay period starting at $t = 500\,\text{ms}$ the preparatory signal (PS) provided either complete or incomplete information about the final movement target and consisted of either a single target LED (Condition 1), two adjacent target LEDs (condition 2), or three adjacent target LEDs (Condition 3) that lit up in green. At $t = 1500\,\text{ms}$ the response signal (RS) appeared and one of the green target LEDs turned red. This indicated the final movement target and prompted the monkey to move his hand to that target. In Conditions 2 and 3 the final target was randomly chosen among the PS-cued targets, while the other target LEDs went dark. The times of movement onset (MO) and movement end (ME) were recorded and if the monkey touched the correct target LED, the trial was registered as successful and a drop of juice was given as a reward. Only successful trials were analyzed in the present study.

The task conditions of one, two or three possible targets presented during the 1s preparatory period were executed in blocks. In each block, 150 trials with randomized target directions were carried out so that each of the directions appeared on average 25 times per condition. Note that in order to obtain the same number of possible trial types in all conditions, not all possible combinations of directions for the preparatory stimulus were used in Conditions 2 and 3. Since six combinations are possible for Condition 1, only the pairs 1-2, 3-4 and 5-6 were used in Condition 2 and for Condition 3, only two cases

occurred (6-1-2, 3-4-5).

Extracellular recordings were obtained with a multielectrode microdrive (Reitböck system; Thomas Recording) to insert transdurally seven independently movable electrodes in the primary motor cortex (M1) close to the central sulcus[32,33]). Online spike sorting resulted in up to seven simultaneously recorded single-unit spike trains[32]. On each recording day, all three conditions were presented to the monkey so that the responses of individual neurons can be compared across conditions.

Model

Spiking network model. Our spiking network model is composed of leaky integrate-and-fire neurons with exponential synaptic currents where the sub-threshold evolution of the membrane potential V is described by the differential equation

$$\frac{dV}{dt} = \frac{-(V - E_L)}{\tau_m} + \frac{I_{syn} + I_x}{C_m}. \tag{3}$$

In the absence of input, the membrane potential decays exponentially to the resting potential E_L with time constant τ_m. The current I_{syn} represents the synaptic input, I_x is an externally injected current and C_m is the membrane capacitance. If the potential reaches the threshold V_{th} a spike is emitted and V is clamped to a reset voltage V_r for an absolute refractory period τ_r. The synaptic current to a neuron i evolves according to the equations

$$\tau_{syn} \frac{dI^i_{syn}}{dt} = -I^i_{syn} + \sum_j J_{ij} \sum_k \delta\left(t - t^j_k\right) \tag{4}$$

where t^j_k is the time of the arrival of the k^{th} spike from presynaptic neuron j and δ is the Dirac delta function.

To facilitate comparison with previous studies that investigated excitatory cluster

topologies we here use similar parameters as provided in Litwin-Kumar et al.[14] and Mazzucato et al.[16] (see Table 1). We briefly explain how we derived the main parameters in the following.

Calibration of the balanced state. We follow the same approach as in Rost et al.[31] for the binary networks by requiring that $\sqrt{K}$ excitatory action potentials arriving within a short time suffice to drive the membrane potential from E_L to V_{th} and hence elicit a spike. For that purpose we need to compute the deflection in the membrane potential caused by a presynaptic spike.

According to equation 4, a spike arriving at $t = 0$ leads to a postsynaptic current of the form

$$I_{psc}(t) = Je^{-t/\tau_{syn}}\,\Theta\,(t) \tag{5}$$

where J and Θ are the synaptic efficacy and step function, respectively. Inserting this into equation 3 and integrating with $V = 0$ at $t = 0$ the postsynaptic potential is obtained:

$$PSP(t) = J\frac{\tau_m\tau_{syn}}{\tau_m - \tau_{syn}}\left(e^{-t/\tau_m} - e^{-t/\tau_{syn}}\right)\Theta\,(t) \tag{6}$$

The maximal deflection PSP_{max} occurs at $t = \frac{log\frac{\tau_{syn}}{\tau_m}}{(1/\tau_m - 1/\tau_{syn})}$. Note that the PSP amplitude depends on the synaptic as well as the membrane time constants and is therefore different for each synapse type (PSP^{EE}_{max}, PSP^{EI}_{max},...). The scale-free weights are then constructed in the same way as for the binary networks (equations 3 to 8 in Rost et al.[31]) but weighted

by the respective PSP amplitudes:

$$j_{EE} = \frac{V_{th} - E_L}{\sqrt{p_{EE} n_E}} \frac{1}{PSP^{EE}_{max}} \tag{7}$$

$$j_{EI} = -g j_{EE} \frac{p_{EE} n_E}{p_{EI} n_I} \frac{PSP^{EE}_{max}}{PSP^{EI}_{max}} \tag{8}$$

$$j_{IE} = \frac{V_{th} - E_L}{\sqrt{p_{IE} n_E}} \frac{1}{PSP^{IE}_{max}} \tag{9}$$

$$j_{II} = -j_{IE} \frac{p_{IE} n_E}{p_{II} n_I} \frac{PSP^{IE}_{max}}{PSP^{II}_{max}} \tag{10}$$

where g is the relative strength of inhibition. The final weights $J_{\alpha\beta}$ are obtained by dividing by $\sqrt{N}$.

Since we are interested in the temporal dynamics of neuronal variability, we modeled external inputs as constant currents to ensure that all variability arises deterministically inside the network rather than stemming from externally generated Poisson input. In analogy to the 'threshold rate' of Brunel[13], the external current I_x is expressed in terms of the current required to reach the threshold in the absence of synaptic input:

$$I_{th} = \frac{V_{th} - E_L}{\tau_m} C_m. \tag{11}$$

A complex interplay exists between the E and I firing rates and the magnitude of the external currents to the populations. The tuning of the injected currents required to obtain the desired firing rates of 3 and 5 spikes per second for the E and I populations respectively was therefore achieved by modeling single units with Poissonian inputs mimicking the network input at the target firing rates. The external inputs could then be increased until the modeled units fired on average at the required rates.

Before introducing structured connectivity we first ensured that the network configuration was operating in the asynchronous-irregular (AI) regime. Irregularity was measured using the squared Coefficient of Variation (CV^2) (as explained in the Data analysis section).

Synchrony of measures such as the instantaneous firing rate or the membrane potential in neural networks can be quantified as[64]:

$$\chi = \sqrt{\frac{\sigma^2_{pop}}{\langle \sigma^2_i \rangle}}. \tag{12}$$

Here σ^2_{pop} is the variance of the the population average and $\langle \sigma^2_i \rangle$ is the average over the individual units' variances. The measure gives unity for totally synchronized activity and for asynchronous activity in networks of size N, one expects $\chi \sim \mathcal{O}\left(\frac{1}{\sqrt{N}}\right)$. Since recording all membrane potentials in simulations is computationally expensive, we computed χ on spike counts measured in bins of 20 ms.

It can be seen in Fig. 7 that the networks show the usual characteristics of the balanced state. When excitation dominates, synchronous-regular firing near the saturation rate $1/\tau_r$ is observed. The AI state occurs when g is sufficiently large for inhibition to dominate (Fig. 7a). As in the binary network[31], we choose $g = 1.2$, where $\chi = 0.02 \sim 1/\sqrt{N}$ and $CV^2 = 0.73$ (Fig. 7b). The raster plot shows no discernible structure (Fig. 7c) and the average firing rate is low and constant over time (Fig. 7d). The synaptic currents from excitatory and inhibitory inputs and the external current Ix cancel so that the net input fluctuates around zero (Fig. 7e). Hence, the membrane potentials fluctuate at low values and only occasionally reach the threshold to produce a spike (Fig. 7f). The parameters used for all simulations in this section are summarized in Table 1.

E and E/I-clustered networks. We follow the same connectivity scheme that we introduced for binary networks in our previous work[31]. Briefly, for the E-clustered networks, we first divide the excitatory population into Q equally sized clusters with uniform connection probability. Then, we potentiate the synaptic connection within each cluster by a factor J_+, which we refer to as cluster strength. $J_+ = 1$ represents the random balanced network and the larger J_+, the stronger the weights within the formed clusters.

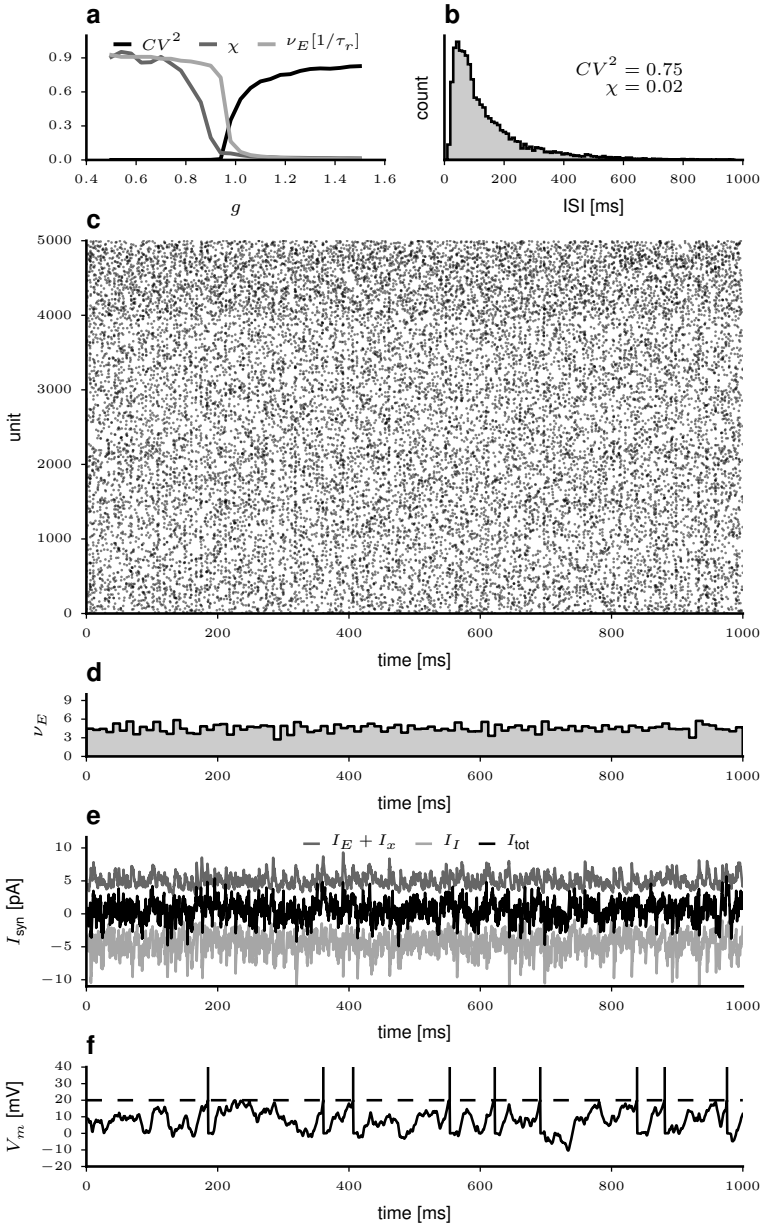

Supplemental Material, Figure 7: Spiking network in the balanced state. Parameters as in Table 1. **a**) Irregularity CV^2, synchrony χ and normalized excitatory firing rate versus relative inhibitory strength g. **b**) Pooled ISI distribution for the E population. **c**) Raster plot of one second of spiking activity for 4000 excitatory (from 0 to 4000) and 1000 (from 4000 to 5000) inhibitory neurons. **d**) E population rate histogram computed in 10 ms bins. **e**) Synaptic currents of a randomly selected E unit. **f**) Membrane potential for same unit as in **e**. Vertical bars above the threshold (dashed line) represent action potentials.

To maintain the overall balance, we decrease the weights among units belonging to different clusters by a factor $J_- = \frac{Q-J_+}{Q-1}$. For the E/I-clustered networks, we divide not only the excitatory population but also the inhibitory population into Q clusters. Then we require that each excitatory cluster selectively influences its corresponding inhibitory cluster and vice versa by increasing the corresponding *EI*, *IE* and *II* weights. We have shown in Rost et al.[31] that the inhibitory clustering needs to be weaker than the excitatory clustering to obtain realistic firing rates. Therefore, we introduce separate excitatory and inhibitory clustering strengths, J_{E+} and J_{E-}. The relation between J_{E+} and J_{E-} is defined as follows:

$$J_{I+} = 1 + R_J(J_{E+} - 1), \tag{13}$$

where R_J is a proportionality factor, i.e. $R_J = 1$ implies the same cluster strength for inhibitory and excitatory clusters ($J_{E+} = J_{I+}$) and $R_J = 0$ makes the inhibitory population unclustered ($J_{I+} = 1$, which represents the E-clustered networks). Throughout the current study, we use $R_J = 3/4$ based on our previous results[31] where we showed that this value of R_J can prevent firing rate saturation in up states.

Attractor model of motor cortex for simulation of the behavioral monkey task. We designed a model with six E/I clusters with 200/50 excitatory/inhibitory neurons each. We adjusted the clustering parameter J_{E+} for the smaller network size to achieve robust metastablity under spontaneous network conditions and an average FF that approximates the average experimental value. The external input currents were slightly adapted to obtain spontaneous firing rates of approximately 3 and 5 spikes per second for excitatory and inhibitory neurons, respectively. No additional parameter tuning was performed and all model parameters are listed in Table 2.

In an ongoing simulation we define successive trials of 2 s length. We randomly define the start of the first trial (TS). This is followed after 500 ms by the onset of the PS and after another 1000 ms by the onset of the RS, which lasted for 400 ms. PS and RS

were realized as constant stimulating currents I_{stim}. After each trial we draw a random inter-trial interval in the range of $1.5 - 1.7$ s before we start the next trial, to allow the network to relax to its spontaneous state. The variance in this relaxation period was intended to avoid any effects of periodicity. For each task condition the model executed 150 trials and for analysis the trials were cut from this long continuous simulation. All analyses of model spiking data were performed identically to the analyses of the *in vivo* spiking data. Our setup implies that each neuron in our model is sharply selective to only a single target direction.

The threshold θ applied to the decision variable DV (equation 2) was adjusted to maximize the performance of the model. The time constant of integration τ_I was set to 50 ms which represents an intermediate value between very fast reactions directly when the threshold is reached at RS and very slow integration where the threshold was not reached during the RS interval.

Data analysis

Quantifying neural variability. The Fano Factor (FF) quantifies the dispersion of spike counts for single neurons across repeated observations of the same experimental condition (trials).

$$FF = \frac{\sigma_c^2}{\mu_c}, \tag{14}$$

where σ_c^2 and μ_c are the variance and mean count over trials. The estimation of the FF is biased towards unity for small estimation windows. However, this bias quickly becomes negligible when the estimation window is several multiples of the mean inter-spike interval (ISI)[65].

To allow a fair comparison of variability statistics across conditions, additional precautions were taken. Fano factors were computed for each unit and direction separately and we required that units had at least ten spikes in the 2 s interval after trial start and that

at least ten trials were recorded per direction. To enable the comparison across conditions, we only included units and directions where those criteria were met in all conditions.

Interval statistics are usually characterized by the Coefficient of Variation (CV) of the ISI distribution,

$$CV^2 = \frac{\sigma^2_{ISI}}{\mu^2_{ISI}}. \tag{15}$$

Here, σ^2_{ISI} and μ_{ISI} are the variance and mean of the intervals between action potentials. Estimating the CV^2 requires some caution, as modulations in firing rate increase the interval variability. Another problem with estimating the CV^2 follows from finite-size estimation windows. In an estimation window of width T, only $ISIs < T$ can be observed. If the underlying process has non-zero probabilities for larger intervals, the CV^2 will be underestimated; this effect is known as right-censoring[35,66]. For estimating the time-varying interval variability we therefore used the CV_2[34,67], which is computed for all pairs of consecutive intervals as:

$$CV_2 = 2 \left\langle \frac{|\tau - \tau'|}{\tau + \tau'} \right\rangle. \tag{16}$$

Here, $\langle ... \rangle$ denotes averaging and τ and τ' are consecutive ISIs.

Decoding of movement direction. To assess how much directional information is contained in the population activity we reproduced the approach of Rickert et al.[33] and constructed pseudo-populations of all available units as follows: the data set was divided into five groups and each group in turn served as the test set while the model was trained on the remaining groups, and the average score of the five models was calculated. At each point in time and using five-fold cross-validation we computed the decoding accuracy of the logistic regression classifier as the fraction of correctly predicted movement directions averaged over all six different directions as

$$\text{Decoding accuracy} = \frac{1}{C} \sum_{c=1}^{C} \frac{N^c_{correct}}{N^c_{total}}. \tag{17}$$

5 Acknowledgments

This project was funded by the German Research Foundation (DFG), in parts through the Collaborative Research Center 'Motor Control in Health and Disease' (DFG-SFB 1451, Project-ID 431549029 to MN) and under the Institutional Strategy of the University of Cologne within the German Excellence Initiative (DFG-ZUK 81/1 to MN and SA). SA received funding through European Union's Horizon 2020 Framework Programme for Research and Innovation under grant agreement number 945539 (Human Brain Project SGA3). We thank Dr. Moritz Deger for fruitful discussions and support in the early phase of the project.

Parameter	Unit	Value
N	-	$4000(E), 1000(I)$
E_L	mV	0
V_{th}	mV	20
V_R	mV	0
C_m	pF	1
τ_m	ms	$20(E), 10(I)$
τ_{syn}	ms	$3(E), 2(I)$
τ_r	ms	5
p_{EE}	-	0.2
p_{EI}, p_{IE}, p_{II}	-	0.5
g	-	1.2
J_{EE}	pA	0.33
J_{EI}	pA	-0.89
J_{IE}	pA	0.25
J_{II}	pA	-1.34
I_x	pA	$2.13I_{th}(E), 1.24I_{th}(I)$

Table 1: Summary of parameters used in the spiking network simulations

Parameter	Unit	Value
N	-	$1200(E), 300(I)$
E_L	mV	0
V_{th}	mV	20
V_R	mV	0
C_m	pF	1
τ_m	ms	$20(E), 10(I)$
τ_{syn}	ms	$3(E), 2(I)$
τ_r	ms	5
p_{EE}	-	0.2
p_{EI}, p_{IE}, p_{II}	-	0.5
g	-	1.2
J_{EE}	pA	0.60
J_{EI}	pA	-1.60
J_{IE}	pA	0.46
J_{II}	pA	-2.44
I_x	pA	$1.25I_{th}(E), 0.78I_{th}(I)$
I_{stim}	pA	0.15
Q	-	6
J_{E+}	-	3.3
R_J	-	3/4

Table 2: Parameters used in the spiking network model for the monkey task

References

1. Renart, A. & Machens, C. K. Variability in neural activity and behavior. *Current opinion in neurobiology* **25**, 211–20 (2014). URL `http://www.sciencedirect.com/science/article/pii/S0959438814000488`.

2. Sakai, K. & Miyashita, Y. Neural organization for the long-term memory of paired associates. *Nature* **354**, 152–155 (1991).

3. Wills, T. J., Lever, C., Cacucci, F., Burgess, N. & O'Keefe, J. Attractor dynamics in the hippocampal representation of the local environment. *Science* **308**, 873–876 (2005).

4. Knierim, J. J. & Zhang, K. Attractor Dynamics of Spatially Correlated Neural Activity in the Limbic System. *Annual Review of Neuroscience* **35**, 267–285 (2012).

5. Miconi, T., McKinstry, J. L. & Edelman, G. M. Spontaneous emergence of fast attractor dynamics in a model of developing primary visual cortex. *Nature Communications* **7**, 1–10 (2016).

6. Pereira, U. & Brunel, N. Attractor Dynamics in Networks with Learning Rules Inferred from In Vivo Data. *Neuron* **99**, 227–238.e4 (2018). URL `https://www.sciencedirect.com/science/article/pii/S0896627318304367?via{%}3Dihub`.

7. Inagaki, H. K., Fontolan, L., Romani, S. & Svoboda, K. Discrete attractor dynamics underlies persistent activity in the frontal cortex. *Nature* **566**, 212–217 (2019).

8. Finkelstein, A. *et al.* Attractor dynamics gate cortical information flow during decision-making. *Nature Neuroscience* 1–8 (2021). URL `https://doi.org/10.1038/s41593-021-00840-6`.

9. Hopfield, J. J. Neural networks and physical systems with emergent collective computational abilities. *Proceedings of the National Academy of Sciences of the United States of America* **79**, 2554–2558 (1982).

10. Amit, D. & Brunel, N. Model of global spontaneous activity and local structured activity during delay periods in the cerebral cortex. *Cerebral Cortex* **7**, 237–252 (1997). URL https://academic.oup.com/cercor/article-lookup/doi/10.1093/cercor/7.3.237.

11. Roudi, Y. & Latham, P. E. A Balanced Memory Network. *PLoS Computational Biology* **3**, e141 (2007). URL https://dx.plos.org/10.1371/journal.pcbi.0030141.

12. van Vreeswijk, C. & Sompolinsky, H. Chaotic balanced state in a model of cortical circuits. *Neural computation* **10**, 1321–71 (1998). URL http://www.ncbi.nlm.nih.gov/pubmed/9698348.

13. Brunel, N. Dynamics of Sparsely Connected Networks of Excitatory and Inhibitory Spiking Neurons. *Journal of Computational Neuroscience* **8**, 183–208 (2000). URL http://link.springer.com/10.1023/A:1008925309027.

14. Litwin-Kumar, A. & Doiron, B. Slow dynamics and high variability in balanced cortical networks with clustered connections. *Nature Neuroscience* **15**, 1498–1505 (2012). URL http://www.nature.com/doifinder/10.1038/nn.3220.

15. Deco, G. & Hugues, E. Neural Network Mechanisms Underlying Stimulus Driven Variability Reduction. *PLoS Computational Biology* **8**, e1002395 (2012). URL http://dx.plos.org/10.1371/journal.pcbi.1002395.

16. Mazzucato, L., Fontanini, A. & La Camera, G. Dynamics of multistable states during ongoing and evoked cortical activity. *The Journal of neuroscience* **35**, 8214–31 (2015). URL http://www.ncbi.nlm.nih.gov/pubmed/26019337http://www.pubmedcentral.nih.gov/articlerender.fcgi?artid=PMC4444543.

17. Mazzucato, L., La Camera, G. & Fontanini, A. Expectation-induced modulation of metastable activity underlies faster coding of sensory stimuli. *Nature Neuroscience* **22**, 787–796 (2019). URL http://www.nature.com/articles/s41593-019-0364-9.

18. La Camera, G., Fontanini, A. & Mazzucato, L. Cortical computations via metastable activity. *Current Opinion in Neurobiology* **58**, 37–45 (2019). 1906.07777.

19. Packer, A. M. & Yuste, R. Dense, unspecific connectivity of neocortical parvalbumin-positive interneurons: a canonical microcircuit for inhibition? *The Journal of neuroscience : the official journal of the Society for Neuroscience* **31**, 13260–71 (2011). URL http://www.ncbi.nlm.nih.gov/pubmed/21917809http://www.pubmedcentral.nih.gov/articlerender.fcgi?artid=PMC3178964.

20. Fino, E. & Yuste, R. Dense inhibitory connectivity in neocortex. *Neuron* **69**, 1188–1203 (2011).

21. Xue, M., Atallah, B. V. & Scanziani, M. Equalizing excitation–inhibition ratios across visual cortical neurons. *Nature* **511**, 596–600 (2014). URL http://www.nature.com/doifinder/10.1038/nature13321.

22. Lee, S.-H. *et al.* Parvalbumin-Positive Basket Cells Differentiate among Hippocampal Pyramidal Cells. *Neuron* **82**, 1129–1144 (2014). URL https://www.sciencedirect.com/science/article/pii/S0896627314003365?via{%}3Dihub.

23. Morishima, M., Kobayashi, K., Kato, S., Kobayashi, K. & Kawaguchi, Y. Segregated excitatoryinhibitory recurrent subnetworks in layer 5 of the rat frontal cortex. *Cerebral Cortex* **27**, 5846–5857 (2017). URL http://academic.oup.com/cercor/article/27/12/5846/4555263.

24. Arkhipov, A. *et al.* Visual physiology of the layer 4 cortical circuit in silico. *PLoS Computational Biology* **14**, e1006535 (2018).

25. Khan, A. G. *et al.* Distinct learning-induced changes in stimulus selectivity and interactions of GABAergic interneuron classes in visual cortex. *Nature Neuroscience* **21**, 851–859 (2018). URL http://www.nature.com/articles/s41593-018-0143-z.

26. Znamenskiy, P. *et al.* Functional selectivity and specific connectivity of inhibitory neurons in primary visual cortex. *bioRxiv* 294835 (2018). URL https://www.biorxiv.org/content/10.1101/294835v2.

27. Shin, M. *et al.* Both excitatory and inhibitory neurons transiently form clusters at the outermost region of the developing mammalian cerebral neocortex. *Journal of Comparative Neurology* **527**, 1577–1597 (2019). URL https://onlinelibrary.wiley.com/doi/abs/10.1002/cne.24634.

28. Najafi, F. *et al.* Excitatory and Inhibitory Subnetworks Are Equally Selective during Decision-Making and Emerge Simultaneously during Learning. *Neuron* **105**, 165 – 179.e8 (2020). URL http://www.sciencedirect.com/science/article/pii/S0896627319308487.

29. Hennequin, G., Agnes, E. J. & Vogels, T. P. Inhibitory Plasticity: Balance, Control, and Codependence. *Annual Review of Neuroscience* **40**, 557–579 (2017). URL https://doi.org/10.1146/annurev-neuro-072116-.

30. Okun, M. & Lampl, I. Instantaneous correlation of excitation and inhibition during ongoing and sensory-evoked activities. *Nature Neuroscience* **11**, 535–537 (2008). URL http://www.nature.com/articles/nn.2105.

31. Rost, T., Deger, M. & Nawrot, M. P. Winnerless competition in clustered balanced networks: inhibitory assemblies do the trick. *Biological Cybernetics* 1–18 (2017). URL http://link.springer.com/10.1007/s00422-017-0737-7.

32. Bastian, A., Schoner, G. & Riehle, A. Preshaping and continuous evolution of motor cortical representations during movement preparation. *European Journal*

of Neuroscience **18**, 2047–2058 (2003). URL http://doi.wiley.com/10.1046/j.1460-9568.2003.02906.x.

33. Rickert, J., Riehle, A., Aertsen, A., Rotter, S. & Nawrot, M. P. Dynamic Encoding of Movement Direction in Motor Cortical Neurons. *Journal of Neuroscience* **29**, 13870–13882 (2009). URL http://www.jneurosci.org/content/29/44/13870.

34. Holt, G. R., Softky, W. R., Koch, C. & Douglas, J. Comparison of discharge variability in vitro and in vivo in cat visual cortex neurons. *Journal of Neurophysiology* **75**, 1806–1814 (1996).

35. Nawrot, M. P. *et al.* Measurement of variability dynamics in cortical spike trains. *Journal of neuroscience methods* **169**, 374–90 (2008). URL http://www.ncbi.nlm.nih.gov/pubmed/18155774.

36. Churchland, M. M., Yu, B. M., Ryu, S. I., Santhanam, G. & Shenoy, K. V. Neural variability in premotor cortex provides a signature of motor preparation. *The Journal of neuroscience : the official journal of the Society for Neuroscience* **26**, 3697–712 (2006).

37. Churchland, M. M. *et al.* Stimulus onset quenches neural variability: a widespread cortical phenomenon. *Nature Neuroscience* **13**, 369–378 (2010). URL http://www.nature.com/articles/nn.2501.

38. Riehle, A., Brochier, T., Nawrot, M. P. & Grün, S. Behavioral Context Determines Network State and Variability Dynamics in Monkey Motor Cortex. *Frontiers in Neural Circuits* **12**, 52 (2018). URL https://www.frontiersin.org/article/10.3389/fncir.2018.00052/full.

39. Churchland, A. *et al.* Variance as a signature of neural computations during decision making. *Neuron* **69**, 818–831 (2011). URL https://www.sciencedirect.com/science/article/pii/S0896627310010871.

40. Isaacson, J. & Scanziani, M. How Inhibition Shapes Cortical Activity. *Neuron* **72**, 231–243 (2011). URL https://www.sciencedirect.com/science/article/pii/S0896627311008798?via{%}3Dihub.

41. Froemke, R. C. Plasticity of Cortical Excitatory-Inhibitory Balance. *Annual Review of Neuroscience* **38**, 195–219 (2015). URL www.annualreviews.org.

42. Van Vreeswijk, C. & Sompolinsky, H. Chaos in neuronal networks with balanced excitatory and inhibitory activity. *Science* **274**, 1724–1726 (1996). URL http://www.ncbi.nlm.nih.gov/pubmed/8939866http://www.sciencemag.org/cgi/doi/10.1126/science.274.5293.1724.

43. Anderson, J. S., Carandini, M. & Ferster, D. Orientation Tuning of Input Conductance, Excitation, and Inhibition in Cat Primary Visual Cortex. *Journal of Neurophysiology* **84**, 909–926 (2000). URL http://www.physiology.org/doi/10.1152/jn.2000.84.2.909.

44. Zhang, L. I., Tan, A. Y. Y., Schreiner, C. E. & Merzenich, M. M. Topography and synaptic shaping of direction selectivity in primary auditory cortex. *Nature* **424**, 201–205 (2003). URL http://www.nature.com/articles/nature01796.

45. Dehghani, N. *et al.* Dynamic Balance of Excitation and Inhibition in Human and Monkey Neocortex. *Scientific Reports* **6**, 23176 (2016). URL http://www.nature.com/articles/srep23176.

46. Rubin, R., Abbott, L. F. & Sompolinsky, H. Balanced excitation and inhibition are required for high-capacity, noise-robust neuronal selectivity. *Proceedings of the National Academy of Sciences of the United States of America* **114**, E9366–E9375 (2017). URL http://www.ncbi.nlm.nih.gov/pubmed/29042519http://www.pubmedcentral.nih.gov/articlerender.fcgi?artid=PMC5676886.

841 47. Nawrot, M. P., Aertsen, A. & Rotter, S. Single-trial estimation of neuronal firing rates:
842 From single-neuron spike trains to population activity. *Journal of Neuroscience Methods*
843 **94**, 81–92 (1999). URL `https://www.sciencedirect.com/science/article/pii/`
844 `S0165027099001272`.

845 48. Gold, J. I. & Shadlen, M. N. The Neural Basis of Decision Making. *Annual Review*
846 *of Neuroscience* **30**, 535–574 (2007). URL `http://www.annualreviews.org/doi/10.`
847 `1146/annurev.neuro.29.051605.113038`.

848 49. Meckenhäuser, G., Krämer, S., Farkhooi, F., Ronacher, B. & Nawrot, M. P. Neural
849 representation of calling songs and their behavioral relevance in the grasshopper
850 auditory system. *Frontiers in Systems Neuroscience* **8**, 183 (2014). URL `http:`
851 `//journal.frontiersin.org/article/10.3389/fnsys.2014.00183/abstract`.

852 50. Kenet, T., Bibitchkov, D., Tsodyks, M., Grinvald, A. & Arieli, A. Spontaneously
853 emerging cortical representations of visual attributes. *Nature* **425**, 954–956 (2003).

854 51. Berkes, P., Orbán, G., Lengyel, M. & Fiser, J. Spontaneous cortical activity reveals
855 hallmarks of an optimal internal model of the environment. *Science* **331**, 83–87 (2011).

856 52. Ponce-Alvarez, A., Nácher, V., Luna, R., Riehle, A. & Romo, R. Dynamics of cortical
857 neuronal ensembles transit from decision making to storage for later report. *Journal*
858 *of Neuroscience* **32**, 11956–11969 (2012).

859 53. Luczak, A., Barthó, P. & Harris, K. D. Spontaneous Events Outline the Realm of
860 Possible Sensory Responses in Neocortical Populations. *Neuron* **62**, 413–425 (2009).

861 54. Teich, M. C., Heneghan, C., Lowen, S. B., Ozaki, T. & Kaplan, E. Fractal character
862 of the neural spike train in the visual system of the cat. *Journal of the Optical Society*
863 *of America A* **14**, 529 (1997).

55. Lagzi, F. & Rotter, S. Dynamics of competition between subnetworks of spiking neuronal networks in the balanced state. *PLoS ONE* **10** (2015).

56. Doiron, B. & Litwin-Kumar, A. Balanced neural architecture and the idling brain. *Frontiers in Computational Neuroscience* **8**, 56 (2014). URL `http://journal.frontiersin.org/article/10.3389/fncom.2014.00056/abstract`.

57. Perin, R., Berger, T. K. & Markram, H. A synaptic organizing principle for cortical neuronal groups. *Proceedings of the National Academy of Sciences of the United States of America* **108**, 5419–5424 (2011).

58. Vogels, T. P., Sprekeler, H., Zenke, F., Clopath, C. & Gerstner, W. Inhibitory plasticity balances excitation and inhibition in sensory pathways and memory networks. *Science* **334**, 1569–1573 (2011). URL `http://science.sciencemag.org/`.

59. Ocker, G. K., Litwin-Kumar, A. & Doiron, B. Self-Organization of Microcircuits in Networks of Spiking Neurons with Plastic Synapses. *PLoS Computational Biology* **11** (2015). `1411.3956`.

60. Zenke, F., Agnes, E. J. & Gerstner, W. Diverse synaptic plasticity mechanisms orchestrated to form and retrieve memories in spiking neural networks. *Nature Communications* **6**, 6922 (2015). URL `http://www.nature.com/articles/ncomms7922`.

61. Litwin-Kumar, A. & Doiron, B. Formation and maintenance of neuronal assemblies through synaptic plasticity. *Nature Communications* **5**, 5319 (2014). URL `http://www.nature.com/articles/ncomms6319`.

62. Mongillo, G., Rumpel, S. & Loewenstein, Y. Inhibitory connectivity defines the realm of excitatory plasticity. *Nature Neuroscience* **21**, 1463–1470 (2018). URL `https://pubmed.ncbi.nlm.nih.gov/30224809/`.

887 63. Wu, Y., Hengen, K. B., Turrigiano, G. G. & Gjorgjieva, J. Homeostatic mechanisms
888 regulate distinct aspects of cortical circuit dynamics. *bioRxiv* 790410 (2019). URL
889 https://www.biorxiv.org/content/10.1101/790410v1.

890 64. Golomb, D. & Hansel, D. The number of synaptic inputs and the synchrony of
891 large, sparse neuronal networks. *Neural Computation* **12**, 1095–1139 (2000). URL
892 http://www.ncbi.nlm.nih.gov/pubmed/10905810.

893 65. Nawrot, M. P. Analysis and interpretation of interval and count variability in neural
894 spikes trains. In Grün, S. & Rotter, S. (eds.) *Analysis of Parallel Spike Trains*, 34–58
895 (Springer Verlag, New York, Berlin, 2010). URL http://www.springerlink.com/
896 index/10.1007/978-1-4419-5675-0.

897 66. Wiener, M. C. An adjustment to the time-rescaling method for application to short-
898 trial spike train data. *Neural computation* **15**, 2565–76 (2003). URL http://www.
899 ncbi.nlm.nih.gov/pubmed/14577854.

900 67. Ponce-Alvarez, A., Kilavik, B. E. & Riehle, A. Comparison of local measures of
901 spike time irregularity and relating variability to firing rate in motor cortical neurons.
902 *Journal of Computational Neuroscience* **29**, 351–365 (2010). URL https://link.
903 springer.com/article/10.1007/s10827-009-0158-2.